ChemComm

# Towards Understanding of Lanthanide-Transition Metal Bonding: Investigations of the First Ce-Fe Bonded Complex



| | |
|---|---|
| Journal: | *ChemComm* |
| Manuscript ID | CC-COM-06-2018-005243.R1 |
| Article Type: | Communication |
| | |

Journal Name

COMMUNICATION

# Towards Understanding of Lanthanide-Transition Metal Bonding: Investigations of the First Ce-Fe Bonded Complex

Received 00th January 20xx,
Accepted 00th January 20xx

DOI: 10.1039/x0xx00000x

www.rsc.org/

Corey P. Burns, Xin Yang, Siyoung Sung, Joshua D. Wofford, Nattami S. Bhuvanesh, Michael B. Hall, and Michael Nippe*

**The syntheses, structural, and magnetic characterization of three new organometallic Ce complexes stabilized by $PyCp_2^{2-}$ ($PyCp_2^{2-}$ = $[2,6\text{-}(CH_2C_5H_3)_2C_5H_3N]^{2-}$) are reported. Complex 1 provides the first example of a crystallographically characterized unsupported Ce-Fe bond in a molecular compound. Results from IR spectroscopy and computational analyses suggest weaker Fe→Ce electron-donation than in a previously reported Dy-Fe bonded species.**

Cerium takes a very special role in the chemistry of the lanthanide (Ln) ions.[1] It is the most abundant member of the Ln series in the earth crust and the Ln-atypical +4 oxidation state is stabilized due to the favorable [Xe]$4f^0$ noble gas configuration of $Ce^{4+}$ such that molecular $Ce^{4+}$ complexes are well known. The $Ce^{3+/4+}$ redox-couple displays unusually high sensitivity to ligand field effects and can span several volts.[2] Recently, $Ce^{3+}$ complexes have been investigated for their photophysical properties and lead to exciting new discoveries of $Ce^{3+}$ species as UVA photosensitizers[3] and potent photoreductants for catalytic organic transformations.[4,5] Another intriguing aspect of $Ce^{3+}$ chemistry is the presence of magnetic anisotropy as consequence of strong spin-orbit coupling. As such, even though the $Ce^{3+}$ ion is an S = 1/2 species, several examples of $Ce^{3+}$ complexes that exhibit field induced slow magnetic relaxation have been reported.[6] Our group is particularly interested in studying magnetization dynamics of lanthanide-transition metal (Ln-TM) bonded complexes[7-11] and we have recently reported a new synthetic approach that allowed us to isolate complexes containing unsupported Dy-Fe and Dy-Ru bonds.[12] In the present work, we show that our synthetic methodology can be successfully applied to the much larger $Ce^{3+}$ ion[13] ($r_{ion}(Dy^{3+})$ = 1.075 Å ; $r_{ion}(Ce^{3+})$ = 1.220 Å) and report the preparation and magnetic characterization of the first complex with an unsupported $Ce^{3+}$-TM bond, (thf)$PyCp_2$Ce-$FeCp(CO)_2$ (**1**). The nature of the Ce-Fe bond is discussed as having highly ionic contributions as judged by $^{57}$Fe Mössbauer and IR spectroscopy as well as QTAIM DFT computational analysis. The structural and magnetic properties of **1** are further compared to those of the new mononuclear complex ($PyCp_2$)Ce($OSO_2CF_3$)(thf) (**3**) and new dinuclear [($PyCp_2$)Ce-(μ-$O_2SOCF_3$)]$_2$ (**2**).

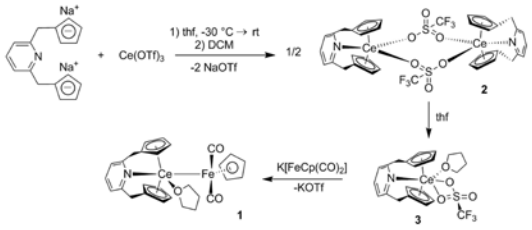


**Scheme 1** Synthesis of **1**, **2**, **3.**

The $PyCp_2^{2-}$ ligand is a rare example of a strongly chelating and structurally rigid binding platform that stabilizes organometallic Ln complexes without introducing significant steric encumbrance around labile coordination sites of the Ln ion and was therefore utilized in the present study. The reaction of anhydrous Ce($OSO_2CF_3$)$_3$ and the disodium salt $Na_2PyCp_2$ yielded dimeric complex [($PyCp_2$)Ce-(μ-$O_2SOCF_3$)]$_2$ (**2**) after crystallization from $CH_2Cl_2$. Complex **2** readily dissociates in thf solvent into monomeric complex ($PyCp_2$)Ce($O_2SOCF_3$)(thf) (**3**) which can be crystallized from thf-hexanes solvent mixtures. The $Ce^{3+/4+}$ redox potentials are known to be strongly dependent on the stabilizing ligand and have been shown to span an unusually large electrochemical potential window.[2] Cyclic voltammograms of **3** in thf solution (Fig. S1) display a single oxidation event at +200 mV ($E_{pa}$ 0.05379 mAcm$^{-2}$ at 1 V/s scan) (vs. $Fc^{0/+}$) which is not reversible at low scan rates (100 mV/s). Increasing the scan rates to values above 1 V/s results in partial recovery of the cathodic current at this potential. These observations suggest that the electrochemically generated oxidized $\mathbf{3}^+$ species is not stable and undergoes fast chemical change (EC mechanism). This irreversibility differs from other organometallic cerium systems like [Ce(COT'')$_2$]$^-$

*Department of Chemistry, Texas A&M University, 3255 TAMU, College Station, TX, 77843 (USA),*
*E-mail: nippe@chem.tamu.edu.*
*Electronic Supplementary Information (ESI) available: Experimental and computational details, X-ray crystallographic data in CIF format, and additional figures and tables. CCDC 1852563, 1852564, 1852566. See DOI: XXXX*

and $[Li(thf)_2Ce(MPB)_2(thf)_2]$ (MPB = 6-*tert*-butyl-4-methylphenolate) which display reversible $Ce^{3+/4+}$ redox couples at -1.43 and -0.93 V.[14,15] It is therefore possible that the oxidation event observed for **3** involves delocalized or ligand based orbitals.

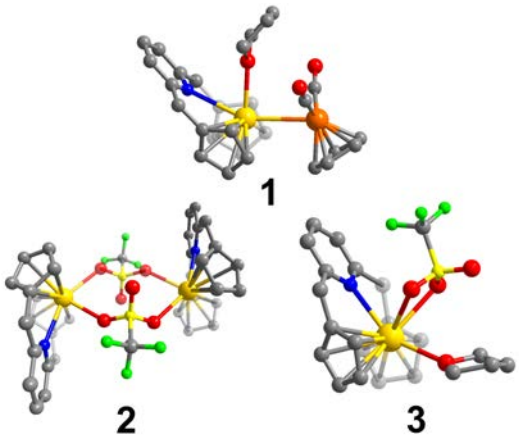


**Fig. 1** Molecular structures of **1**, **2**, and **3**. Hydrogen atoms have been omitted for clarity. The color scheme is as follows: gray = carbon, red = oxygen, blue = nitrogen, green = fluorine, light yellow = sulfur, orange = iron, golden yellow = cerium.

The weakly binding triflate anion of **3** is a good leaving group and allows for its facile substitution by $[FeCp(CO)_2]^-$ in the reaction of **3** with stoichiometric amounts of $K[FeCp(CO)_2]$ in thf at low temperatures to yield crystalline material of the Ce-Fe bonded complex $(thf)PyCp_2Ce\text{-}FeCp(CO)_2$ (**1**).

The molecular structures of compounds **1**, **2**, and **3** were investigated by means of single crystal x-ray diffraction studies (Fig. 1, Table S1, S2). While the Ce-C distances are similar in **1** (2.759(2) – 2.827(2) Å), **2** (2.730(2) – 2.794(2) Å), and **3** (2.712(4) – 2.825(4) Å) the Ce-N distance in **1** (2.779(2) Å) is significantly longer than that in **2** (2.621(2) Å) and **3** (2.618(3) Å). There are several structural differences observed between the mononuclear $Ce^{3+}$ complexes **1** and **3** as compared to their previously reported $Dy^{3+}$ analogues $\mathbf{1_{Dy}}$ and $\mathbf{3_{Dy}}$.[16] The binding of the triflate anion in **3** involves close interactions with two of the triflate O-atoms ($d(Ce\text{-}O_{triflate})$ =2.697(3), 2.749(3) Å) while only one $Dy\text{-}O_{triflate}$ interaction (2.335(1) Å) was observed in $\mathbf{3_{Dy}}$. In comparing the Ln-Fe bonded complexes **1** and $\mathbf{1_{Dy}}$, we notice that the increase in ionic radius[8] (1.075 Å for $Dy^{3+}$ to 1.220 Å for $Ce^{3+}$) allows for the additional binding of a thf molecule to Ce. The Ce-Fe distance in **1** (3.1546(5) Å) is longer than the Dy-Fe distance in $\mathbf{1_{Dy}}$ (2.884(2) Å) and is to the best of our knowledge the first structurally characterized unsupported direct bond between an iron ion and a formally $Ce^{3+}$ ion. The binding of an additional thf solvent molecule to Ce in **1** also affects the coordination environment of the Fe ion. While the $Fe\text{-}C_{Cp}$ and $Fe\text{-}C_{CO}$ distances in **1** (2.109[2] Å and 1.733(2) Å) and $\mathbf{1_{Dy}}$ (2.10[1] Å and 1.716(9) Å) are comparable, the $\sphericalangle(Ln\text{-}Fe\text{-}Cp_{centroid})$ (121.8° in **1**; 105.9° in $\mathbf{1_{Dy}}$) and $\sphericalangle(C_{CO}\text{-}Fe\text{-}C_{CO})$ (95.4° for **1**; 89.4° for $\mathbf{1_{Dy}}$) angles differ significantly.

These structural differences around the Fe site have direct consequences for the spectroscopic parameters of **1**. The $^{57}Fe$ Mössbauer spectrum of **1** (Fig. S2) at 4.6 K indicates a single component with an isomershift ($\delta$) of 0.133 mm/s and a quadrupole splitting ($\Delta E_Q$) of 2.075 mm/s, while we previously found $\delta$ = 0.129 mm/s and $\Delta E_Q$ = 1.859 mm/s for $\mathbf{1_{Dy}}$ at 5 K. The significant difference in $\Delta E_Q$ (between **1** and $\mathbf{1_{Dy}}$) is in agreement with the high sensitivity of $\Delta E_Q$ to changes in the geometry of the electric field gradient around the Fe nucleus. However, given the above discussed structural variations we cannot include a direct comparison of the values of $\delta$ of **1** and $\mathbf{1_{Dy}}$ into the comparative discussion of the strength of electron donation from Fe→Ce or Fe→Dy.

The solid-state IR spectra of Ce-Fe bonded **1** (Fig. S3) feature CO stretching modes at 1890 and 1814 $cm^{-1}$ which are at lower energies than the CO stretching frequencies in the Dy-Fe analogue $\mathbf{1_{Dy}}$ (1910, 1840 $cm^{-1}$). This observation suggests stronger Fe-CO π-backbonding interactions in **1** as compared to $\mathbf{1_{Dy}}$ and would therefore also imply higher electron density on the Fe site in **1**, which in turn could be a result of smaller Fe→Ce donor interactions in **1** as compared to Fe→Dy interactions in $\mathbf{1_{Dy}}$. Indeed, this interpretation is further supported by our computational analysis.

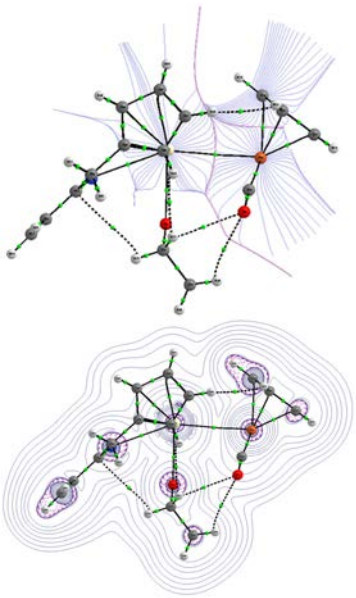

**Fig. 2** Top: Basin paths with Interatomic Surface (IAS) paths. Bottom: Contour Plots of $\nabla^2\rho$.

To gain computational insight into the nature of the Ce-Fe bond in **1**, we followed the frequently employed QTAIM[17] approach utilizing Gaussian G09-D01[18-20], BP86/Ce, cc-pVTZ-DK3 (all electron) Fe, cc-pVTZ-DK (all electron) C, N, O, H, 6-311G*, Orca 4.0.0[21], (single point and geometry optimizations with the ZORA Hamiltonian; BP86/Ce, SARC-ZORA-TZVP; Fe, C, N, O, H, ZORA-def2-TZVP), and ADF[22] (single point and geometry optimizations with the ZORA Hamiltonian, BP86/TZ2P). The computational results following either single point calculations based on the experimental crystal structure or after full geometry optimization are summarized in Table S3 and are almost identical to each other, independent of the approach. We readily identify a line critical point (lcp) between Ce and Fe

which is slightly more proximal to Fe than to Ce (d(Ce-lcp) = 1.60 Å; d(Fe-LCP) = 1.55 Å), which is in contrast to the perfectly central position of the lcp between Dy and Fe in $\mathbf{1_{Dy}}$. Another striking difference between **1** and $\mathbf{1_{Dy}}$ is the much lower calculated delocalization index (DI) of 0.35 for the Ce-Fe bond in **1** (DI(Dy-Fe in $\mathbf{1_{Dy}}$) = 0.45). This result supports the formulation of weaker Fe→Ce donation in **1** as compared to Fe→Dy donation in $\mathbf{1_{Dy}}$ and is therefore in agreement with lower energy CO stretching frequencies in **1** as compared to $\mathbf{1_{Dy}}$.

Although $Ce^{3+}$ is an S = 1/2 species, strong spin-orbit coupling results in significant magnetic anisotropy and can lead to slow magnetic relaxation for $Ce^{3+}$ complexes. Previously reported mononuclear $Ce^{3+}$ complexes display solely field-induced slow magnetic relaxation[23,24] and only one example of a linear, trinuclear Zn(II)-Ce(III)-Zn(II) complex[25] has exhibited slow magnetic relaxation in the absence of static fields. We therefore investigated the static and dynamic magnetic properties of complexes **1**, **2**, and **3**. The temperature dependence of the molar magnetic susceptibility temperature product ($\chi_M T$) using a 1000 Oe direct current (dc) field are shown in Figures S4-6. The experimental room temperature $\chi_M T$ values of 0.71 (for **1**), 1.63 (for **2**), and 0.75 (for **3**) emu $mol^{-1}$ K are close to the expected values of 0.80 and 1.60 emu $mol^{-1}$ K for one (**1** and **3**) or two (**2**) non-interacting $Ce^{3+}$ ions ($^2F_{5/2}$, S = 1/2, L = 3, J = 5/2, and g = 6/7). All three complexes exhibit decreases in $\chi_M T$ with decreasing temperature, typically observed and attributed to thermal depopulation of Stark sublevels in $Ce^{3+}$. All three complexes also exhibit a slight increase in $\chi_M T$ at 2 K, which could possibly be indicative of weak intermolecular ferromagnetic interactions.

Variable temperature magnetization (M) versus field (H) measurements (see Fig. S7-9 for M vs. H; Fig. S10-12 for M vs. H/T) indicate that compounds **1**, **2**, and **3** do not reach magnetic saturation even up to fields of 7 T (M at 1.8 K: 0.75 (for **1**), 1.48 (for **2**), and 0.62 $\mu_B$ (for **3**)). Although the M vs. H/T plots appear to be fairly superimposable, the lack of magnetic saturation would be in agreement with some amount of magnetic anisotropy which is consistent with the dynamic magnetic measurements discussed below.

In the absence of applied dc fields, none of the three investigated complexes exhibited signals in the out-of-phase component of the alternating current (ac) magnetic susceptibility (χ'') at temperatures of 3 or 2 K. However, application of dc fields resulted in signals with well-defined maxima in χ'' at temperatures below 4 K for all three complexes (Figures S13-18). Fits of the resulting Cole-Cole plots (Figures S19-21) to the generalized Debye equation resulted in the dc field-dependence of the magnetic relaxation times τ for **1**, **2**, and **3** (Figures S22-24). All three complexes exhibit a typical initial increase of magnetic relaxation times with increasing field up to an optimal dc field, followed by decrease in τ values at higher fields. This behaviour can be interpreted by an initial decrease of contributions from quantum tunnelling of the magnetization (QTM) to relaxation, followed by introduction of field-induced direct processes at higher fields. The optimal dc fields differ strongly for the three complexes (500 Oe for **1**, 1500 Oe for **2**, 4000 Oe for **3**), and interestingly is the smallest for Ce-Fe bonded complex **1**. The optimal field for Dy-Fe bonded $\mathbf{1_{Dy}}$ was previously reported as 1500 Oe. The field dependence of τ was fitted to equation 1: $\tau^{-1} = AH^{n_1}T + \frac{B_1}{1+B_2H^2} + D$ . Here, A represents the direct relaxation parameter, $B_1$ and $B_2$ are QTM parameters, and D accounts for Orbach and Raman contributions which are field independent.[27]

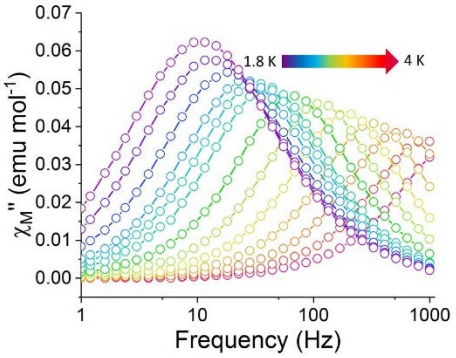


**Fig. 3** Out-of-phase ($\chi_m''$) component of the ac susceptibility of **1** between 1.8 K – 4 K ($H_{dc}$ = 500 Oe).

Constraining $n_1$ to a value of 4, the value expected for a Kramers ion in the absence of hyperfine interactions[28] (I = 0 for all Ce isotopes), we observe the fitting values for each parameter as shown in Table S4. Fig. 3 (for **1**) and Fig. S28 and S29 for (**2** and **3**) show the temperature dependence of $\chi_M''$ signals conducted at the individual optimal dc fields of each complex (see Fig. S25-27 for $\chi_M'$). Extraction of the relaxation times from the corresponding Cole-Cole plots (Fig. S30-32) allowed to generate the Arrhenius plots shown in Fig. 4. It should be mentioned that for compound **3** the appearance of a second, slower relaxation process was observed at temperatures below 2.4 K. Although both processes could be fitted using the CC fit software,[29] we only show the τ values associated with the faster process for **3** in Fig. 4. There are multiple approaches to estimating an effective energy barrier ($U_{eff}$) to magnetization reversal from Arrhenius plots. The linear regime of the temperature dependent part of the Arrhenius plot can be fitted to estimate Ueff, by assuming

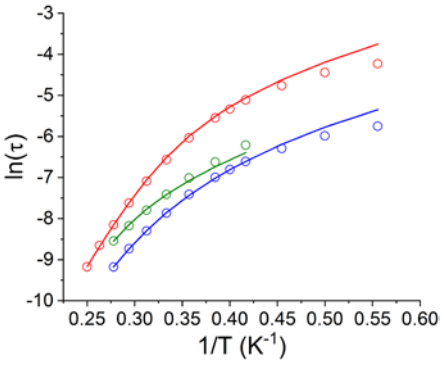


**Fig. 4** Arrhenius plot of magnetization relaxation times for **1** (red), **2** (blue), and **3** (green) under optimal dc fields. Open circles correspond to experimental data, whereas the lines correspond to the fit according to equation 3.

that magnetic relaxation occurs solely via the Orbach mechanism, using equation 2: $\tau^{-1} = \tau_0^{-1} \cdot \exp(-U_{eff}/k_BT)$ (Fig. S33). The calculated barriers are 33 $cm^{-1}$, 24 $cm^{-1}$, and 21 $cm^{-1}$ with $\tau_0$ values of $2.71 \cdot 10^{-8}$ s, $1.51 \cdot 10^{-7}$ s, and $5.85 \cdot 10^{-7}$ s for compounds **1**, **2**, and **3**, respectively. Alternatively, the data can be fit over the whole experimental temperature range according equation 3:

$$\tau^{-1} = AH^4T + \tau_{QTM}^{-1} + CT^{n2} + \tau_0^{-1}\exp(^{-U}/_{k_BT}) \cdot$$

In the fitting routine, we restricted $n_2$ to a value of 5, which is the expected value for a Kramers ion with low lying excited states,[23] and the values for A, $B_1$, and $B_2$ were restrained to the above determined values from the dc field dependence of $\tau$ to avoid over parameterization. According to this model, we obtained U values of 29 $cm^{-1}$, 28 $cm^{-1}$, and 38 $cm^{-1}$ with associated $\tau_0$ values of $3.50 \cdot 10^{-9}$ s, $3.02 \cdot 10^{-9}$ s, and $1.66 \cdot 10^{-10}$ s for compounds **1**, **2**, and **3**, respectively. Although the here reported U values are similar to other cerium compounds that exhibit field induced slow magnetic relaxation, we are hesitant to make direct comparisons as the reported examples did not account for direct relaxation processes in the fit equation. Independent of the exact U values, we can summarize the dynamic magnetization properties and note that the dc field dependence of the three complexes varies significantly (with **1** showing the lowest optimal dc fields) and that under optimal dc fields, Ce-Fe bonded complex **1** displays longer relaxation times at a given temperature. These findings may suggest that the incorporation of Ln-TM bonding could contribute to future SMM design guidelines.

M.N. is grateful for support of this project by the National Science Foundation (CHE-1753014) and general financial support through The Welch Foundation (A-1880). M.B.H. acknowledges support from the National Science Foundation (CHE-1664866) and The Welch Foundation (A-0648). The High Performance Research Computing Facility and the Laboratory for Molecular Simulation at TAMU provided computer time and software. We thank B. Foley, A. Kosanovich, and O. Ozerov for their help in obtaining IR spectra. $^{57}$Fe Mössbauer spectra were acquired on instruments in the Dr. P. A. Lindahl research group (NIH, GM127021).

## Conflicts of interest

There are no conflicts to declare.

## Notes and references

1 R. Anwander, M. Dolg, F. T. Edelmann, *Chem. Soc. Rev.*, 2017, **46**, 6697-6709.
2 N. A. Piro, J. R. Robinson, P. J. Walsh, E. J. Schelter, *Coord. Chem. Rev.*, 2014, **260**, 21-36.
3 H. Yin, Y. Jin, J. E. Hertzog, K. C. Mullane, P. J. Carroll, B. C. Manor, J. M. Anna, E. J. Schelter, *J. Am. Chem. Soc.*, 2016, **138**, 16266-16273.
4 Y. Qiao, Q. Yang, E. J. Schelter, *Angew. Chem. Int. Ed.*, 2018, *Accepted*
5 H. Yin, P. J. Carroll, B. C. Manor, J. M. Anna, E. J. Schelter, *J. Am. Chem. Soc.*, 2016, **138**, 5984-5991.
6 F. Pointillart, O. Cador, B. Le Guennic, L. Ouahab, *Coord. Chem. Rev.*, 2017, **346**, 150-175.
7 I. P. Beletskaya, A. Z. Voskoboynikov, E. B. Chuklanova, N. I. Kirillova, A. K. Shestakova, I. N. Parshina, A. I. Gusev, G. K. I. Magomedov, *J. Am. Chem. Soc.*, 1993, **115**, 3156-3166.
8 M. V. Butovskii, O. L. Tok, F. R. Wagner, R. Kempe, *Angew. Chem. Int. Ed.*, 2008, **47**, 6469-6472.
9 P. L. Arnold, J. McMaster, S. T. Liddle, *Chem. Commun.*, 2009, 818-820.
10 M. P. Blake, N. Kaltsoyannis, P. Mountford, *J. Am. Chem. Soc.*, 2011, **133**, 15358-15361.
11 M. V. Butovskii, R. Kempe, New. J. Chem., 2015, 39, 7544-7558.
12 C. P. Burns, X. Yang, J. D. Wofford, N. S. Bhuvanesh, M. B. Hall, M. Nippe, *Angew. Chem. Int. Ed.*, 2018, **57**, 8144-8148.
13 P. D'Angelo, A. Zitolo, V. Migliorati, G. Chillemi, M. Duvail, P. Vitorge, S. Abadie, R. Spezia, *Inorg. Chem.*, 2011, **50**, 4572-4579.
14 B. D. Mahoney, N. A. Piro, P. J. Carroll, E. J. Schelter, *Inorg. Chem.*, 2013, **52**, 5970-5977.
15 J. J. Le Roy, I. Korobkov, J. E. Kim, E. J. Shelter, M. Murugesu, *Dalton. Trans.* 2014, **43**, 2737-2740.
16 C. P. Burns, B. O. Wilkins, C. M. Dickie, T. P. Latendresse, L. Vernier, K. R. Vignesh, N. S. Bhuvanesh M. Nippe, *Chem. Commun.*, 2017, **53**, 8419-8422.
17 R. F. W. Bader, *Chem. Rev.*, 1991, **91**, 893–928.
18 Gaussian 09, Revision D.01, M. J. Frisch et al., Gaussian, Inc., Wallingford CT, **2009**.
19 (a) J. P. Perdew, *Phys. Rev. B* 1986, **33**, 8822-8824; (b) A. D. Becke, *Phys. Rev. A* 1988, **38**, 3098-3100.
20 (a) N. Balabanov, K. A. Peterson, *J. Chem. Phys.*, 2005, **123**, 064107-1- 064107-15; (b) Q. Lu and K. A. Peterson, *J. Chem. Phys.*,2016, **145**, 054111-1-054111-13; (c) K. Raghavachari, J. S. Binkley, R. Seeger, and J. A. Pople, *J. Chem. Phys.*, 1980, **72**, 650-654.
21 (a) *ORCA 4.0.0*, WIREs Comput Mol Sci 2018, 8:e1327; (b) E. van Lenthe, E. J. Baerends, J. G. Snijders, *J. Chem. Phys.*, 1993, **99**, 4597-4610; (c) D. A. Pantazis, X. Y. Chen, C. R. Landis, F. Neese, *J. Chem. Theory Comput.*, 2008, **4**, 908-919.
22 (a) G.te Velde, F.M. Bickelhaupt, E.J. Baerends, C. Fonseca Guerra, S.J.A. van Gisbergen, J.G. Snijders, T. Ziegler, *J. Comput. Chem.*, 2001, **22**, 931-967; (b) C. Fonseca Guerra, J.G. Snijders, G. te Velde and E.J. Baerends, *Theor. Chem. Acc.*, 1998, **99**, 391-403; (c) *ADF2017*, *SCM*, *Theoretical Chemistry*, Vrije Universiteit, Amsterdam, The Netherlands, http://www.scm.com; (d) E. van Lenthe, E. J. Baerends, *J. Comput. Chem.* 2003, **24** , 1142–1156.
23 H. Wada, S. Ooka, T. Yamamura, T. Kajiwara, *Inorg. Chem.*, 2017, **56**, 147-155.
24 A. Upadhyay, K. R. Vignesh, C. Das, S. K. Singh, G. Rajaraman, M. Shanmugam, *Inorg. Chem.*, 2017, **56**, 14260-14276.
25 S. Hino, M. Maeda, K. Yamashita, Y. Kataoka, M. Nakano, T. Yamamura, H. Nojiri, M. Kofu, O. Yamamuro, T. Kajiwara, *Dalton Trans.*, 2013, **42**, 2683-2686.
26 S.-D. Jiang, B.-W. Wang, G. Su, Z.-M. Wang and S. Gao, *Angew. Chem. Int. Ed.*, 2010, **49**, 7448–7451.
27 C. M. Dickie, A. L. Laughlin, J. D. Wofford, N. S. Bhuvanesh, M. Nippe, *Chem. Sci.*, 2017, **8**, 8039-8049.
28 S. T. Liddle, J. van Slageren, *Chem. Soc. Rev.*, 2015, **44**, 6655-6669.
29 N. F. Chilton, *CC Fit*, The University of Manchester, United Kingdom, 2014.

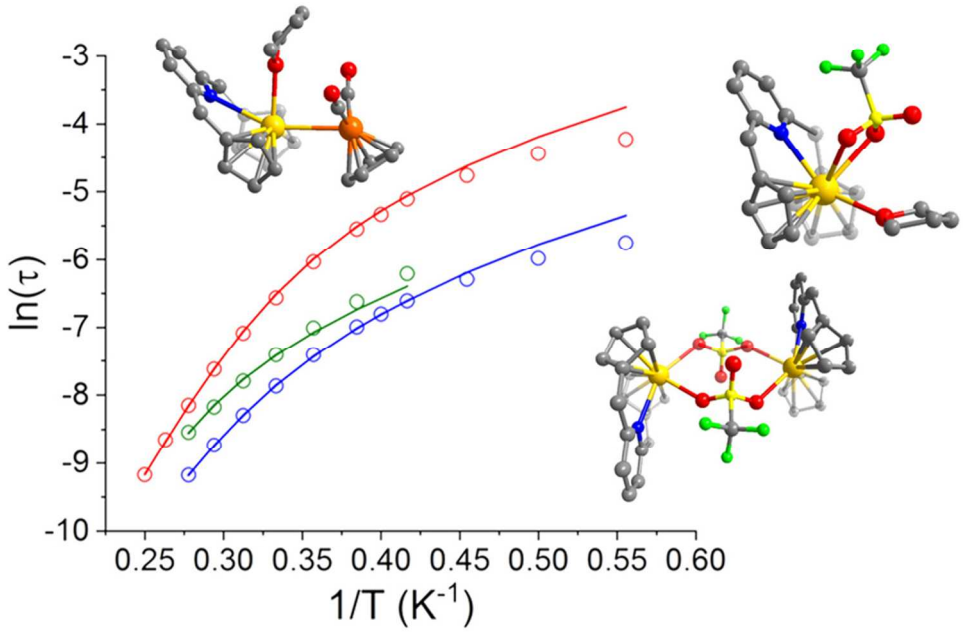


40x27mm (600 x 600 DPI)